Unifying Lengthscale-Based Rheology of Dense Granular-Fluid Mixtures

Zhuan Ge,[1,2] Teng Man,[2,*] Herbert E. Huppert,[3] Kimberly Hill,[4,†] and Sergio Andres Galindo-Torres[2,‡]

[1] *College of Civil Engineering and Architecture, Zhejiang University, 866 Yuhangtang Road, Hangzhou 310058, Zhejiang, China*

[2] *Key Laboratory of Coastal Environment and Resources of Zhejiang Province (KLaCER), School of Engineering, Westlake University, 18 Shilongshan Street, Hangzhou, Zhejiang 310024, China.*

[3] *Institute of Theoretical Geophysics, King's College, University of Cambridge, King's Parade, Cambridge CB2 1ST, United Kingdom*

[4] *Department of Civil, Environmental, and Geo-Engineering, University of Minnesota, Minneapolis, Minnesota, USA*

(Dated: May 11, 2023)

In this communication, we present a new lengthscale-based rheology for dense sheared particle suspensions as they transition from inertial- to viscous-dominated. We derive a lengthscale ratio using physics-based considerations for a particle subjected to pressure and drag. In doing so, we demonstrate that an appropriately derived length-scale ratio provides a consistent relationship between normal stress and system proximity to its "jammed" or solid-like state, even as a system transitions between inertial and viscous states, intrinsically captured by a variable Stokes number.

Particle flows and particle-fluid flows are ubiquitous in natural phenomena, such as landslides, debris flows, and rock falls [1–3] Complex environmental conditions make it difficult to obtain a unified constitutive law for their flow characteristics, particularly for dense flows, where short-range interactions are enduring and often generate long-range correlations[4].

In the last two decades, significant progress has been made in modeling the flows of wet and dry granular flows, focused on dimensional analysis and time scales. For dry granular flows, the local normal stress P_p (which is associated with interparticle interactions only), particle density ρ_s, particle size d, and shear rate $\dot{\gamma}$ are combined into a single dimensionless ratio of two timescales, microscopic ($\sqrt{\rho_s d^2/P_p}$) and macroscopic ($1/\dot{\gamma}$): $I = \dot{\gamma} d/\sqrt{P_p/\rho_s}$ [5–7]. Various authors have shown that dynamic parameters such as the apparent friction coefficient $\mu = \tau/P_p$ (here, τ is a local shear stress) and the solid fraction ϕ can be represented using functions of I in both steady-state [5] and transient (e.g., column collapse) systems [8]. Cassar et al.[9] adapted this framework to saturated particle systems by replacing the microscopic (inertial) timescale with a viscous timescale (η_f/P_p, where η_f is the fluid viscosity), and the appropriate dimensionless control parameter is $J = \dot{\gamma}\eta_f/P_p$. Boyer et al.[10] further validated the saturated framework and generalized the form to include much sparser suspensions.

In the last decade, work on dense flows has broadened to include systems in which both fluid viscous forces and particle inertial effects contribute to the rheology. Towards this, Trulsson et al. (2012) [11] proposed an effective shear stress in the form of a linear superposition of inertial and viscous stresses ($\tau_{\text{eff}} = \lambda \times \rho_s d^2\dot{\gamma}^2 + \eta_f\dot{\gamma}$ normalized by P_p yielding a new dimensionless number: $K = \lambda I^2 + J$ (λ is a single-valued fit parameter). Based on their experimental data, Tapia et al.[12] argued that $\lambda = 1/St_{\text{tr}}$, where St_{tr} is a transitional Stokes number ($St = I^2/J$) close to 1. They found that they needed *two* fitted numbers, to collapse their μ and ϕ data ($St_{\text{tr},\mu} = 114$ and $St_{\text{tr},\phi} = 10$, respectively).

These efforts have revolutionized the representation of dense granular-fluid flows. Nevertheless, significant issues remain, associated with issues of material properties [12, 13] and representations of transitions from inertial-dominated to viscous-dominated dynamics [14]. Recent rheologies based on combinations of I and J include static fitted variables to transition from $I-$ to $J-$ dominated behaviors [11, 12, 15].

In this communication, we address these points by deriving a new lengthscale-based rheology for dense sheared flows based on the ratio of average relative ("macroscopic") displacements (associated with streamwise travel in the shearing direction) to deviations from those displacements. The latter ("microscopic" displacements), increasingly restricted relative to the streamwise displacements as the system ϕ approaches its maximum value ϕ_c. We start by using a conceptualized model to show how near= ϕ_c dynamics are partially represented in increasingly limited streamwise-normal movements (compared to streamwise movements) as the system deviates from ϕ_c. Then, we theoretically derive the appropriate lengthscale ratio between average displacements and average variants from those displacements to model how the ratio varies with solid and fluid properties and forcing conditions. This gives rise to a rheological parameter that requires *no* additional fit parameters and includes a function of the Stokes number St_{tr} that varies through the inertial-to-viscous transition, intrinsically capturing the transition at varying ϕ/ϕ_c proximities to 1 [16]. We demonstrate that the new framework contextualizes previously proposed timescale based frameworks, and also fits published experimental and compu-

* manteng@westlake.edu.cn
† kmhill@umn.edu
‡ s.torres@westlake.edu.cn

tational data[10, 12, 15, 17, 18], and new computational data presented herein.

We begin with a conceptual model of one particle among a conglomeration of particles sheared under uniform shear and normal stresses τ and P_p (Fig. 1). For a shear rate of $\dot{\gamma}$, the average streamwise velocity between particles in layer $i+1$ and i is $\approx d\dot{\gamma}$. During the *macroscopic* timescale $1/\dot{\gamma}$ our particle in layer $i+1$ (A in Fig. 1(b)) moves streamwise by $\approx d$. It also moves down and up in the $y-$direction, a distance "δ", e.g., Fig. 1(b) to 1(d). When $\dot{\gamma}$ is relatively low and P_p high, a particle in layer $i+1$ remains in contact with particles in layer i and it travels a maximun vertical distance (2δ, Fig. 1(c)). In contrast, when P_p is low and $\dot{\gamma}$ is high, we expect our particle A to break contact with particle B in layer i before connecting with C, reducing the value for 2δ, e.g., Fig. 1(b) to 1(d). Overall, this framework provides insight that while streamwise particle travel is relatively free, the $y-$direction travel is spatially-limited, and likely directly related to solid fraction ϕ, particularly in dense sheared flows. This suggests the importance of displacement lengthscales in capturing their rheology. (See the supplement for related effects on ϕ and μ.)

We next derive a quantitative expression for what we might call a "microscopic" lengthscale l_μ in the context of representative forces on a particle. This is analogous to δ, as conceptualized above, though the direction of l_μ is arbitrary. As previously noted [9], when inertia, drag force, and P_p are all significant, we may write:

$$(\pi/6)\rho_s d^3 \frac{dv}{dt} = (\pi/4)P_p d^2 - F_d, \tag{1}$$

for the response of a particle to a contact force on one side (scaling with P_p), in a viscous fluid, with no particle contact on the other side (e.g., due to a "hole" in the contact network). We approximate the drag force by the Stokes force, $F_d = 3\pi\eta_f v d$ (and discuss this simplification shortly). We integrate Eqn. 1 to find the speed $v(t)$ and distance travelled $l(t)$ for a particle released from rest:

$$v(t) = \int_{t'=0}^{t} [dv(t')/dt']dt' = v_\mathrm{f}(1 - e^{-t/t_0}), \tag{2a}$$

$$l(t) = \int_{t'=0}^{t} v(t')dt' = v_\mathrm{f}t - v_\mathrm{f}t_0(1 - e^{-t/t_0}). \tag{2b}$$

$v_\mathrm{f} = Pd/(12\eta_\mathrm{f})$ is analogous to a settling velocity, and $t_0 = (\rho_s d^2)/18\eta_f$, to a settling timescale. We can use Eqn. 2b to derive either a "microscopic timescale" t_μ for a particle to travel distance $l = d$ or a "microscopic lengthscale" l_μ a particle can travel in time $\mathcal{T} = 1/\dot{\gamma}$:

$$t_\mu = \frac{12\eta_f}{P_p} + \frac{\rho_s d^2}{18\eta_f}\left[1 + W\left(-e^{-216\eta_f^2/(\rho_s d^2 P_p)-1}\right)\right] \tag{3a}$$

$$l_\mu = \frac{P_p d}{(12\eta_\mathrm{f})\dot{\gamma}} - \frac{P_p d^3 \rho_s}{216\eta_\mathrm{f}^2}(1 - e^{-18\eta_f/(\rho_s d^2\dot{\gamma})}) \tag{3b}$$

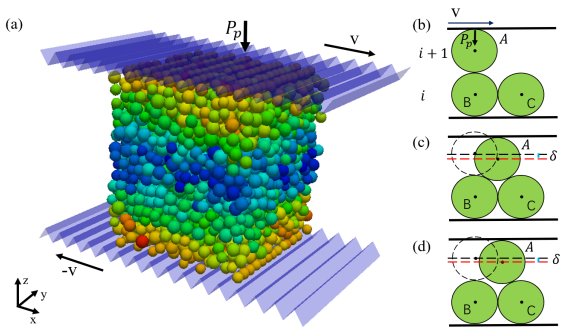

FIG. 1. (a) Planar shear simulation setup. The top plate exerts a pressure P_p on the particles while the granular assembly is sheared by the top and bottom plates under the same velocity v in the opposite direction. (b) Schematic of a 2-D conceptual model of a particle in layer $i+1$ subjected to shear and normal stresses over particles in layer i. (c) Relative motion for low $\dot{\gamma}$ (and/or high P_p). (d) Relative motion for higher $\dot{\gamma}$ (and/or lower P_p).

where $W(\cdot)$ is the Lambert-W function. (See supplement for calculation details.)

With these, we find a dimensionless timescale ratio by dividing t_μ by the ("macroscopic") timescale $\mathcal{T} = 1/\dot{\gamma}$:

$$\Gamma = \frac{t_\mu}{\mathcal{T}} = 12J + \frac{\mathrm{St}}{18}\left[1 + W\left(-e^{-216J/\mathrm{St}-1}\right)\right] \tag{4}$$

and a dimensionless lengthscale ratio by dividing a ("macroscopic") lengthscale $\mathcal{L} = d$ by l_μ:

$$G = \frac{\mathcal{L}}{l_\mu} = \frac{216J^2}{18J - I^2(1 - e^{-18/\mathrm{St}})} = 12(J + \lambda_\mathrm{St} I^2); \tag{5a}$$

$$\lambda_\mathrm{St} = \frac{(1 - e^{-18/\mathrm{St}})}{18 - \mathrm{St} \times (1 - \mathrm{e}^{-18/\mathrm{St}})}. \tag{5b}$$

To lend perspective into these new ratios (Γ and G), we summarize some details in Table I including their relationships with I, J, and K. The first column details conditions for comparisons (i.e., high and low St and in between). The second column summarizes previously published relationships for I, J, and K. In the third and fourth columns, we see that in the high-St limits, Γ and $\sqrt{G}$ scale identically with I. However, at the lowest values of St , Γ scales with J, while $\sqrt{G}$ scales with $\sqrt{J}$ suggesting the need for an additional fit parameter may be needed for Γ to fully reconcile with the data. In fact, the form of G is similar to K with an important difference which will be highlighted later on.

We use a 3D Discrete Element Method (DEM) simulation to produce data together with previously published simulation and experimental data to compare the relative effectiveness of the three functions formulated to capture the rheology over the full St range: K, G, and Γ (Figs. 2-3). Our DEM model uses previously

TABLE I. Near$-\phi_c$ dynamics and rheological parameters for viscous to inertial behaviors ($St \approx 0 \rightarrow \infty$)

Flow regimes	$I,\ J,\ K$ relationships	$\Gamma = t_f/\mathcal{T}$	$G = \mathcal{L}/l$
Inertial (St $\rightarrow \infty$)	$(\frac{\phi_c}{\phi} - 1) \propto I \propto \frac{\dot{\gamma}}{\sqrt{P_p}}$ [5–7]	$(\frac{\phi_c}{\phi} - 1) \propto \lim_{\mathrm{St/J}\rightarrow\infty} \Gamma = \frac{2}{\sqrt{3}} I$	$(\frac{\phi_c}{\phi} - 1) \propto \lim_{St\rightarrow\infty} \sqrt{G} = \frac{2}{\sqrt{3}} I$
Viscous (St $\rightarrow 0$)	$(\frac{\phi_c}{\phi} - 1) \propto \sqrt{J} \propto \sqrt{\frac{\dot{\gamma}}{P_p}}$ [9, 10]	$(\frac{\phi_c}{\phi} - 1) \propto \lim_{\mathrm{St/J}\rightarrow 0} \sqrt{\Gamma} = \sqrt{12J}$	$(\frac{\phi_c}{\phi} - 1) \propto \lim_{St\rightarrow 0} \sqrt{G} = \sqrt{12J}$
Visco-inertial[a,b] ($\mathrm{St} \approx 0 \rightarrow \infty$)	$\phi_c - \phi \propto \sqrt{K}$ [11, 12] $(\frac{\phi_c}{\phi} - 1) \propto \sqrt{K}$ [15]	$(\frac{\phi_c}{\phi} - 1) \propto \Gamma^{\alpha_\Gamma}$ $\alpha_\Gamma = 0.5 \rightarrow 1$	$(\frac{\phi_c}{\phi} - 1) \propto G^{\alpha_G}$ $\alpha_G = 0.5$

[a] $K = \lambda_i I^2 + J$; where λ_i is a fit parameter that can have two values, one each for $i = \phi$ or μ [12];
[b] Γ and G are in Eqns. 4-5a. α_Γ is a fit parameter for Γ. No fit parameters are needed for G.

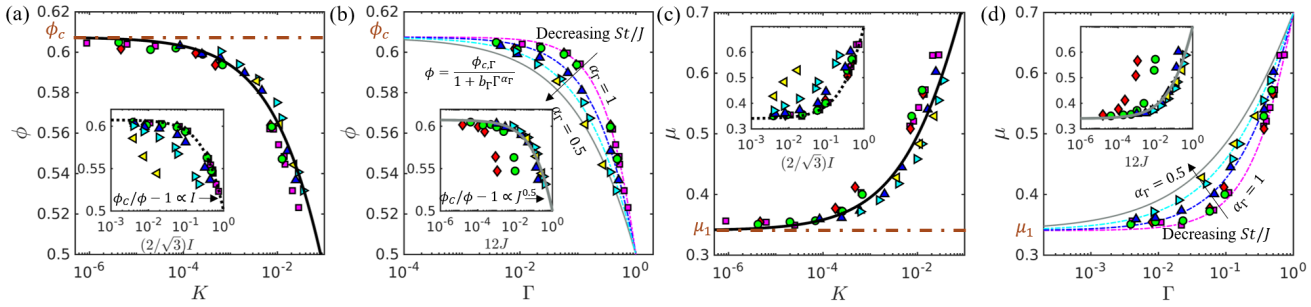

FIG. 2. DEM data for ϕ and μ plotted vs. K and Γ for particles submerged in fluids of different viscosities [η_f =0.1 cP ($\Diamond$), 1 cP ($\bigcirc$), 20 cP (Δ), 100 cP ($\triangleright$), 10^3 cP ($\triangleleft$), and 0 ($\square$)]. (a) ϕ vs. $K = J + \lambda_o I^2$, with $\lambda_o = 0.1$, (inset ϕ vs. $2I/\sqrt{3}$). (b) ϕ vs. $t_\mu/\mathcal{T} = \Gamma$ (inset ϕ vs. $12J$). (c) μ vs. K (inset μ vs. $(2/\sqrt{3})I$). (d) μ vs. Γ (inset μ vs. $12J$), The lines are fit to the data using Eqn. 6a-6b. The fit parameters for $\mathcal{X} = K$ in (a) and (c) are in Table 2. The fit parameters for $\mathcal{X} = \Gamma$ in (b) and (d) and insets are as follows: $[\phi_{c,\mathcal{X}}, b_\mathcal{X}, \mu_{1,\mathcal{X}}, \mu_{2,\mathcal{X}}, Q_\mathcal{X}]$=[0.6075, 0.215, 0.34, 1.49, 2.2], and α_Γ decreases with decreasing St/J as shown.

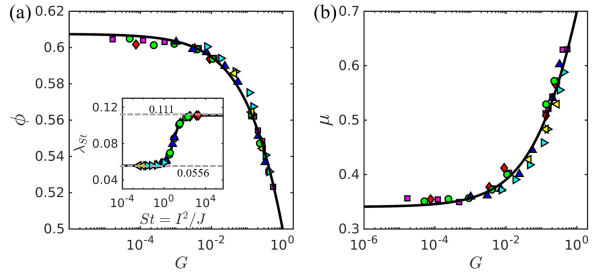

FIG. 3. (a) ϕ and (b) μ plotted vs. the length scale G. The solid lines in (a) and (b) are fitted by Eqs.6a and 6a, respectively. Inset of (a) shows λ vs. St (Eqn.5b).

published relationships for (1) linear interparticle contact forces [19], (2) a viscous (Stokes) fluid drag[11], and (3) lubrication forces[13, 20] (details in the supplement). Each simulation uses 2800 spheres whose radii are uniformly distributed between 0.07−0.1 cm. Particle density ρ_s= 1.18 g/cm^3; normal and tangential stiffnesses are 5×10^7 dyn/cm, and 2.5×10^7 dyn/cm, respectively, and their restitution and frictional coefficients are 0.2 and 0.3, respectively. Our particles are bounded by two rough plates normal to the $z-$ direction and periodic boundaries in both $x-$ and $y-$ directions (Fig.1(a)). The two plates move with equal and opposing $x-$ velocities. The bottom plate is fixed in the $z-$direction, while the $z-$position of the top plate adjusts to exert constant P_p on the particles. From one simulation to the next, we vary the dynamics via: $\dot{\gamma}$ = 0.15 to 50 s^{-1}, P_p = 80 to 300 Pa, and η_f = 0.1 to 1000 cP. We calculate the interparticle stress tensor σ_{ij} through all contact pairs [21] and, from this, P_p, τ, and μ. ϕ is the sum of all particle volumes divided by the cell volume. For both σ_{ij} and ϕ we exclude regions adjacent to the plates to avoid associated inhomogeneities.

We assess the rheological parameters for each system once it reaches a steady state, (details in the supplementary document). We then plot μ and ϕ vs. each of K, Γ, or G (Figs. 2-3). In all three cases, the data can be fitted reasonably well by previously proposed relationships:

$$\mu(\mathcal{X}) = \mu_{1,\mathcal{X}} + \frac{\mu_{2,\mathcal{X}} - \mu_{1,\mathcal{X}}}{1 + \mathcal{Q}_\mathcal{X}/\mathcal{X}^{\alpha_\mathcal{X}}}, \text{and} \tag{6a}$$

$$\phi(\mathcal{X}) = \frac{\phi_{c,\mathcal{X}}}{1 + b_\mathcal{X}\mathcal{X}^{\alpha_\mathcal{X}}}. \tag{6b}$$

Here, $\phi_{c,\mathcal{X}}$, $b_\mathcal{X}$, $\mu_{1,\mathcal{X}}$, $\mu_{2,\mathcal{X}}$, $\alpha_\mathcal{X}$ and $\mathcal{Q}_\mathcal{X}$ are fit parameters for each rheological parameter (e.g., Table.II) and each fit parameter ξ delineated with subscript $\mathcal{X}$, i.e., "$\xi_\mathcal{X}$" refers to fit parameter ξ obtained using $\mathcal{X} = K, \Gamma$, or G in fitting Eqns. 6a-6b to the data (Tab II; we include fitting methodology in the Supplement). The form of μ indicates there is a lower and higher limit for μ associated with quasistatic and kinetic limits, respectively[7]. The

form of ϕ indicates only an upper limit for the dense flows, similar to a random close-packed configuration. Best fit coefficients μ_1, μ_2, and ϕ_c are similar for K, Γ, and G, consistent with their relationship to fundamental properties of the systems [13]. While the quality of fit is similarly good for all, without a closed form for the exponent α_Γ, which we have shown must change from 0.5 to 1, we find Γ impractical and do not consider it further herein. In contrast, G does not require such solutions since $\alpha_G = 0.5$ for all cases.

As a further test of G we consider previously published experimental and computational data [10, 12, 17, 18] for μ and ϕ. Considering μ_1, μ_2, and ϕ_c as constants for each particle-fluid system [22], we normalize the μ and ϕ data and plot them vs. G ($\tilde{\mu}$ and $\tilde{\phi}$ in Fig. 4). We overlay these data with the fitted relationship we found for our new data (Fig. 3) and find all data collapse and are fit remarkably well by the same dimensionless relationships. What determines the apparent universality for $\mathcal{Q}_G$ in μ and b_G in all of these systems is beyond the scope of this communication, though we are currently pursuing this issue. This means the scaling laws of μ and ϕ can be represented by a single dimensionless number $G(\dot{\gamma}, P_p, d, \rho_s, \eta_f)$ in a fluid-granular system. Additionally, these results lend further credence to the significance of normalizing μ and ϕ using system-dependent values of ϕ_c, μ_1, μ_2 [22], results that require further investigation to be fully understood. Finally, this work eliminates the need for additional fitting parameters, e.g., λ_ϕ and λ_μ as expressed in [12], which uses $K(\dot{\gamma}, P_p, d, \rho_s, \eta_f, \lambda_\phi, \lambda_\mu)$. The RMSE of prediction of μ for their data decreases significantly from 1.9e-2 to 8.2e-5 using Eqn.6a.

Before we conclude, we briefly revisit the question of appropriate system scales. As we recall, I and J were derived using ratios of macro- to micro- timescales for inertial and viscous systems, respectively, while the intentionally-designed cross-rheology parameter K was initially proposed based on a linear superposition of stress scales.[11] (similar to $I_m = \sqrt{\alpha_1 I^2 + \alpha_2 J}$[15]). Starting from these superpositions ends with forms that require additional fit parameters (λ_o or λ_μ and λ_ϕ for K or α_1/α_2 for I_m). Our new timescale ratio Γ provides a generalized form of J and I from viscous regime to inertial regime. However, it still requires a fit parameter α, that varies from 1/2 to 1 as the system transitions from viscous to inertial (Table I). Our new lengthscale ratio G does not require a fitting parameter, and, at the same time, it contains the functional form of $\lambda(St)$ necessary to transform G into K (Eq.5b). The lenghtscale can more effectively capture the evolution of macroscopic properties of the granular assembly. The importance of lengthscales is highlighted by the proposed conceptual model. We elaborate on additional relationships between lengthscale ratio and macroscopic properties ϕ and μ through this conceptual model along with force analysis and geometric operation (See supplementary materials.)

In addition to the rheological studies reviewed here, studies of near-jammed (near ϕ_c) systems have illustrated

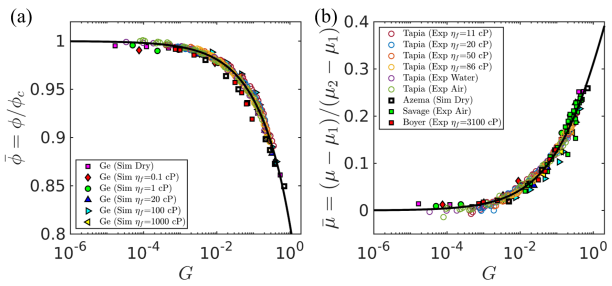

FIG. 4. Normalized solid fraction (a) and apparent frictional coefficient (b) plotted vs. data from G for data from Refs.[10, 12, 17, 18]. The solid line in (a) and (b) are from Eqns.6a and 6b, using b_G and $\mathcal{Q}_G$ from our data (Table 2).

that spatial structures play an important role during particle transport (e.g., Refs. [16, 23, 24]. For example, the dynamical processes of granular flows are strongly correlated to larger-scale correlated movements within a granular assembly. While the relationships between the structures and flows remain open questions, we have provided significant justifications to give renewed importance to the proposed lengthscale ratios over the existing alternatives.

To summarize, in this communication, we considered the inertial response of a sphere subjected to contact pressure P_p and a linear drag force, and derived a particle-response micro-timescale $t_\mu = t(l = d)$ and equivalent micro-lengthscale $l_\mu = l(t = 1/\dot{\gamma})$ (i.e., the time for a particle to travel by d and the distance for a particle to travel in time $1/\dot{\gamma}$, respectively, in response to this forcing). From these, we derived a timescale ratio and a lengthscale ratio: $\Gamma = t_\mu/(1/\dot{\gamma})$ and $G = d/l_\mu$. When considering these in the context of new and previously published data, we found that the lengthscale ratio (rather than a timescale ratio) is intrinsically related to the rheology and requires no additional fitting parameters in comparison with existing alternatives. Based on these results along with recent work connecting particle properties with rheology parameters [22], we propose general constitutive relationships suitable for a wide range of dense, sheared granular flows across the viscous-inertial transition expressed using dimensionless scales G and St where the effects of viscous drag and inertia change under different confining pressures, fluid viscosities, and macroscopic deformations. These results provide insight toward expanding our understanding of the

TABLE II. Regression analysis for the expression of μ and ϕ.

Expression	Fitting parameter	R-Square	RMSE
$\phi_c/(1 + b\sqrt{G})$	b, ϕ_c=0.215,0.6075	0.99	3.0e-3
$\phi_c/(1 + b\sqrt{K})$	b, ϕ_c=0.826,0.6072	0.95	5.8e-3
$\mu_1 + \frac{\mu_2 - \mu_1}{1+\mathcal{Q}/\sqrt{G}}$	$\mathcal{Q}$,μ_1,μ_2=2.2, 0.34, 1.49	0.97	1.6e-2
$\mu_1 + \frac{\mu_2 - \mu_1}{1+\mathcal{Q}/\sqrt{K}}$	$\mathcal{Q}$,μ_1,μ_2=0.45, 0.34, 1.29	0.91	2.8e-2

influence of different lengthscales in dense particle-fluid flows, providing greater promise for formulating constitutive models for larger-scale physics-based flow for larger scales than the ones we explored herein.

This work is supported by the National Natural Science Foundation of China (NSFC grants NO. 12172305 and NO. 12202367) and the US National Science Foundation under grant number EAR-2127476. We thank Westlake High Performace Computing Center for computational resources and related assistance. The simulations were based on the MECHSYS open source library (`http://mechsys.nongnu.org`).

[1] K. Hutter, T. Koch, C. Pluüss, and S. B. Savage, The dynamics of avalanches of granular materials from initiation to runout. part ii. experiments, Acta Mechanica **109**, 127 (1995).
[2] P. Tegzes, T. Vicsek, and P. Schiffer, Avalanche dynamics in wet granular materials, Physical Review Letters **89**, 094301 (2002).
[3] G. C. Yang, L. Jing, C. Y. Kwok, and Y. D. Sobral, Pore-scale simulation of immersed granular collapse: Implications to submarine landslides, Journal of Geophysical Research: Earth Surface **125** (2020).
[4] K. Kamrin, Non-locality in granular flow: Phenomenology and modeling approaches, Frontiers in Physics **7**, 116 (2019).
[5] G. MiDi, On dense granular flows, The European Physical Journal E **14**, 341 (2004).
[6] F. da Cruz, S. Emam, M. Prochnow, J.-N. Roux, and F. Chevoir, Rheophysics of dense granular materials: Discrete simulation of plane shear flows, Physical Review E **72**, 021309 (2005).
[7] P. Jop, Y. Forterre, and O. Pouliquen, A constitutive law for dense granular flows, Nature **441**, 727 (2006).
[8] L. Lacaze and R. R. Kerswell, Axisymmetric granular collapse: a transient 3d flow test of viscoplasticity, Physical Review Letters **102**, 108305 (2009).
[9] C. Cassar, M. Nicolas, and O. Pouliquen, Submarine granular flows down inclined planes, Physics of fluids **17**, 103301 (2005).
[10] F. Boyer, É. Guazzelli, and O. Pouliquen, Unifying suspension and granular rheology, Physical Review Letters **107**, 188301 (2011).
[11] M. Trulsson, B. Andreotti, and P. Claudin, Transition from the viscous to inertial regime in dense suspensions, Physical Review Letters **109**, 118305 (2012).
[12] F. Tapia, M. Ichihara, O. Pouliquen, and E. Guazzelli, Viscous to inertial transition in dense granular suspension, Physical Review Letters **129**, 078001 (2022).
[13] T. Man, Q. Feng, and K. Hill, Rheology of thickly-coated granular-fluid systems, arXiv preprint arXiv:1812.07083 (2018).
[14] R. A. Bagnold, Experiments on a gravity-free dispersion of large solid spheres in a newtonian fluid under shear, Proceedings of the Royal Society of London. Series A. Mathematical and Physical Sciences **225**, 49 (1954).
[15] L. Amarsid, J.-Y. Delenne, P. Mutabaruka, Y. Monerie, F. Perales, and F. Radjai, Viscoinertial regime of immersed granular flows, Physical Review E **96**, 012901 (2017).
[16] L. Bocquet, A. Colin, and A. Ajdari, Kinetic theory of plastic flow in soft glassy materials, Physical review letters **103**, 036001 (2009).
[17] S. B. Savage, The mechanics of rapid granular flows, Advances in Applied Mechanics **24**, 289 (1984).
[18] E. Azéma and F. Radjaï, Internal structure of inertial granular flows, Phys. Rev. Lett. **112**, 078001 (2014).
[19] P. A. Cundall and O. D. Strack, A discrete numerical model for granular assemblies, Geotechnique **29**, 47 (1979).
[20] A. J. Goldman, R. G. Cox, and H. Brenner, Slow viscous motion of a sphere parallel to a plane wall—i motion through a quiescent fluid, Chemical engineering science **22**, 637 (1967).
[21] I. Goldhirsch and C. Goldenberg, On the microscopic foundations of elasticity, The European Physical Journal E **9**, 245 (2002).
[22] T. Man, P. Zhang, Z. Ge, S. A. Galindo-Torres, and K. M. Hill, Friction-dependent rheology of dry granular systems, Acta Mechanica Sinica **39**, 1 (2023).
[23] J. Choi, A. Kudrolli, R. R. Rosales, and M. Z. Bazant, Diffusion and mixing in gravity-driven dense granular flows, Physical review letters **92**, 174301 (2004).
[24] C. Bonnoit, J. Lanuza, A. Lindner, and E. Clement, Mesoscopic length scale controls the rheology of dense suspensions, Physical review letters **105**, 108302 (2010).
[25] H. M. Jaeger, S. R. Nagel, and R. P. Behringer, Granular solids, liquids, and gases, Reviews of modern physics **68**, 1259 (1996).
[26] J.-N. Roux and G. Combe, Quasistatic rheology and the origins of strain, Comptes Rendus Physique **3**, 131 (2002).
[27] I. Goldhirsch, Rapid granular flows, Annual review of fluid mechanics **35**, 267 (2003).
[28] T. C. Scott, R. Mann, and R. E. Martinez Ii, General relativity and quantum mechanics: towards a generalization of the lambert w function a generalization of the lambert w function, Applicable Algebra in Engineering, Communication and Computing **17**, 41 (2006).
[29] D. Veberič, Lambert w function for applications in physics, Computer Physics Communications **183**, 2622 (2012).
[30] C. Ness and J. Sun, Flow regime transitions in dense nonbrownian suspensions: Rheology, microstructural characterization, and constitutive modeling, Physical Review E **91**, 012201 (2015).
[31] E. DeGiuli, G. Düring, E. Lerner, and M. Wyart, Unified theory of inertial granular flows and non-brownian suspensions, Physical Review E **91**, 062206 (2015).

Unifying Lengthscale-Based Rheology of Dense Granular-Fluid Mixtures: Supplementary Material

Zhuan Ge,[1,2] Teng Man,[2,*] Herbert E. Huppert,[3]
Kimberly Hill,[4] and Sergio Andres Galindo-Torres[2,†]

[1] *Zhejiang University, 866 Yuhangtang Road, Hangzhou 310058, Zhejiang, China*

[2] *Key Laboratory of Coastal Environment and Resources of Zhejiang Province (KLaCER), School of Engineering, Westlake University, 18 Shilongshan Street, Hangzhou, Zhejiang 310024, China.*

[3] *Institute of Theoretical Geophysics, King's College, University of Cambridge, King's Parade, Cambridge CB2 1ST, United Kingdom*

[4] *Department of Civil, Environmental, and Geo-Engineering, University of Minnesota, Minneapolis, Minnesota, USA*

(Dated: May 11, 2023)

In this supplementary material, we provide more detail on several issues mentioned in the main text. Following the order as we mention them in the manuscript:

- we provide clarifying details of the derivation of the time scale ratio Γ and the length scale ratio G;
- we use a conceptual model to express the physical relationships between length scale ratio G and macroscopic properties: ϕ and μ;
- we demonstrate the relationships among the characteristic rheology scalars previously proposed (the inertial number I, the viscous number J, and the visco-inertial number K) and those proposed here for the first time (the time scale ratio Γ, the length scale ratio G);
- we provide details of the force model we use in the new DEM simulations;
- we demonstrate how we perform regression analysis to determine the fit coefficients for μ and ϕ
- we demonstrate how that G is an appropriate rheology variable for 2-d simulated data and other experimental and simulated data, provided appropriate granular materials properties are included in the fits. , and
- we provide the materials properties for those previously published data – specifically, critical solid fractions and apparent frictional coefficients.

TIME SCALE RATIO Γ AND LENGTH SCALE RATIO G

To derive the new time scale ratio we propose in this Letter, as discussed briefly in the main text, we first solve the momentum equation of a sphere of diameter d moving downward at a speed $v(t)$ in a fluid of dynamic viscosity η:

$$(\pi/6)\rho_s d^3 \frac{dv}{dt} = F_{\Delta P} - F_d. \tag{1}$$

Here, the forces on the right-hand side are due to a local typical pressure gradient and a drag force. The pressure forces associated with a constant pressure gradient P_p for a particle of diameter d: $F_{\Delta P} = P_p(\pi/4)d^3$ We approximate the hydrodynamic force as the Stokes drag

force $F_d = 3\pi\eta_f v d$. We assumed a linear drag force, which is a simplification of the complex interactions that occur in real granular materials. However, this assumption is a common one in computational studies of dense granular materials (where the Reynolds number is relatively low.)[1], and it allows us to gain insight into the behavior of these materials in a controlled and systematic way. In a granular system with loose packing, an even more complete approach may indeed require that one considers a transition between drag at low Reynolds numbers and a drag at higher Reynolds numbers. Then, when released from rest at time $t = 0$, we find the velocity of the particle, $v(t) = v_f(1 - e^{-at})$, where

$$a = 18\eta_f/(\rho_s d^2), \text{ and} \tag{2a}$$

$$v_f = P_p d^2/(12\eta_f) \tag{2b}$$

is an effective terminal velocity, at which the hydrodynamic force balances the inertial force. After time t, after releasing from rest, the distance the sphere has traveled is

$$z = \int_0^t v(t)dt = v_f t - \frac{v_f}{a}(1 - e^{-at}) \tag{3}$$

essentially Equation [2b] in the main text. Here, we provide more detail for the reader to connect these results to the final expressions for Γ and G. For convenience, with some algebra we can rewrite this equality as

$$a\left(t_\mu - \frac{1}{a} - \frac{z}{v_f}\right)\exp\left[a\left(t_\mu - \frac{1}{a} - \frac{z}{v_f}\right)\right] = -\exp\left[-\left(1 - \frac{az}{v_f}\right)\right]. \tag{4}$$

Eqn.4 has the form of the Lambert W-function, $Xe^X = Y$, and X can be calculated using the Lambert W-function W as $X = W(Y)$ [2]. Hence, the solution for t_μ is expressed as

$$t_\mu = \frac{z}{v_f} + \frac{1}{a} + \frac{1}{a}W\left(-e^{\frac{-az}{v_f}-1}\right) = \frac{12\eta_f}{P_p} + \frac{\rho_s z^2}{18\eta_f}\left[1 + W\left(-e^{-216\eta_f^2/(\rho_s z^2 P_p)-1}\right)\right]. \tag{5}$$

As defined by Cassar et al. (2005)[3], the microscopic characteristic time scale t_μ is the time it takes for a particle traveling for a distance of d. Substituting d for z in Eqn. 5, we obtain

$$t_\mu = \frac{12\eta_f}{P_p} + \frac{\rho_s d^2}{18\eta_f}\left[1 + W\left(-e^{-216\eta_f^2/(\rho_s d^2 P_p)-1}\right)\right]. \tag{6}$$

This is identical to Equation [3a] in the main text.

The ratio $\Gamma = \frac{t_\mu}{\mathcal{T}}$, between the microscopic time scale t_μ and macroscopic rearrangement time scale $\mathcal{T} = 1/\dot{\gamma}$ is

$$\begin{aligned}\Gamma &= 12J + \frac{I^2}{18J}\left[1 + W\left(-e^{-\frac{216J^2}{I^2}-1}\right)\right] \\ &= 12J\left[1 + \frac{St}{216J} + \frac{St}{216J}W\left(-e^{-\frac{216J}{St}-1}\right)\right] \\ &= \frac{2I}{\sqrt{3}}\left[6\sqrt{3}\sqrt{\frac{J}{St}} + \frac{\sqrt{3}}{36}\sqrt{\frac{St}{J}} + \frac{\sqrt{3}}{36}\sqrt{\frac{St}{J}}W\left(-e^{-\frac{216J}{St}-1}\right)\right],\end{aligned} \tag{7}$$

where $St = I^2/J = \frac{\rho_s \dot{\gamma} d^2}{\eta_f}$, $St/J = \frac{P_p \rho_s d^2}{\eta_f^2}$.

As we demonstrated in the text, we found the most effective rheological relationships to be based on the length scale ratio we derived using analogous steps:

$$G = \frac{216J^2}{18J - I^2(1 - e^{-18J/I^2})}, \tag{8}$$

To see how this may be rewritten in the form we presented in the main paper, we first substitute $A = (1 - e^{-18J/I^2})$ to simplify our presentation. Using this, we obtain

$$\begin{aligned}G &= \frac{216J^2}{18J - AI^2} \\ &= \frac{12J(18J - AI^2) - 12J(18J - AI^2) + 216J^2}{18J - AI^2} \\ &= 12J + \frac{216J^2 - 12J(18J - AI^2)}{18J - AI^2} \\ &= 12J + \frac{12AJI^2}{18J - AI^2} \\ &= 12\left(J + \frac{A}{18 - AI^2/J}I^2\right) \\ &= 12\left[J + \frac{1 - e^{-18J/I^2}}{18 - (1 - e^{-18J/I^2})I^2/J}I^2\right]\end{aligned} \tag{9}$$

This expression is equivalent to:

$$G = 12(J + \lambda(\mathrm{St})\mathrm{I}^2), \text{where} \tag{10a}$$

$$\lambda(\mathrm{St}) = \frac{1 - \mathrm{e}^{-18/\mathrm{St}}}{18 - \mathrm{St} \times (1 - \mathrm{e}^{-18/\mathrm{St}})} \tag{10b}$$

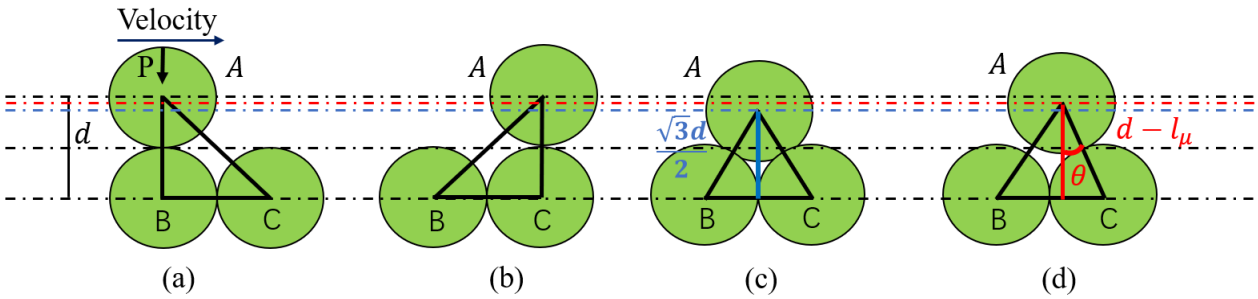

FIG. 1. Schematic showing the physical meaning of the length scale ratio.

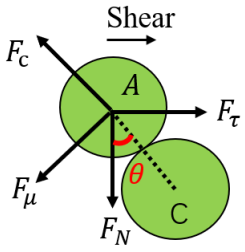

FIG. 2. Force analysis of the particles during shearing in the condition as shown in figure.1(d).

RELATIONSHIPS BETWEEN THE LENGTH SCALE RATIO AND MACROSCOPIC PROPERTIES OF GRANULAR MATERIALS: ϕ AND μ VS G

We use a conceptual model to illustrate relationships between the length scale ratio and macroscopic properties: the solid fraction and apparent frictional coefficient. As shown in Fig.1, during the shearing process, the two layers of particles have a velocity gradient $\dot{\gamma} = (v_A - v_B)/d$, after a rearrangement time $1/\dot{\gamma}$. Particle A will cross the top of particle C when particle displacement in vertical direction $l_\mu \ll d$ as shown in Fig.1(b). When $l_\mu \gg d$, particles A, B, and C will generate dense packing $\phi_c = V_p/V_s$, where V_p is the sum area of the three particles in 2-D condition (due to the volume of particles is constant, we assume $V_p = 1$), $V_s = \sqrt{3}d^2/4$ is the area of the space, we use the area of the triangle of the three particles to represent as shown in Fig.1(c). A more general expression of the solid fraction is expressed as $V_s = d(d - l_\mu)/2$ as shown in Fig.1(d). Hence, the solid fraction is given by:

$$\frac{\phi}{\phi_c} = \frac{\sqrt{3}d^2/4}{d(d - l_\mu)/2} = \frac{\sqrt{3}}{2(1 - \frac{l_\mu}{d})} = f(l_\mu/d) = f(G) \tag{11}$$

As shown in Fig.2, we assume that in the quasi-steady state, momentum transport can

be expressed by: $F_N = \pi d^2 P/4$ at the vertical direction and $F_\tau = \pi d^2 \tau/4$ at the shearing direction. The frictional force between particle A and C is $F_\mu = \mu_p F_c$, where F_c is the contact force and μ_p is the particle frictional coefficient of the particles. Hence, we can obtain

$$F_c cos\theta - \mu_p F_c sin\theta = F_N = \pi d^2 P/4 \tag{12a}$$

$$F_c sin\theta - \mu_p F_c cos\theta = F_\tau = \pi d^2 \tau/4 \tag{12b}$$

The apparent frictional coefficient μ can be expressed

$$\mu = \frac{\tau}{P} = \frac{F_\tau}{F_N} = \frac{\sin\theta + \mu_p \cos\theta}{\cos\theta - \mu_p \sin\theta} = \frac{\tan\theta + \mu_p}{1 - \mu_p \tan\theta} \tag{13a}$$

$$\tan\theta = \frac{\sqrt{d^2 - (d - l_\mu)^2}}{d - l_\mu} = \sqrt{\left(\frac{1}{1 - l_\mu/d}\right)^2 - 1} = g(G) \tag{13b}$$

Hence, we can express the apparent frictional coefficient $\mu = f(G, \mu_p)$ and the solid fraction $\phi = g(G, \phi_c)$ by the length scale ratio. Although the dynamic process of granular material during shearing is much more complex, this simplified conceptual model still provides physical insight into the behavior of granular materials and allows us to use G to build a ϕ-based rheological model.

RELATIONSHIPS AMONG RHEOLOGICAL VARIABLES: G AND Γ VS. I, J, K

The relationship between G and K is apparent. The expressions are nearly identical, except for the need for a fitting parameter λ. In the case of K, $\lambda = \lambda_o$, is a constant that needs to be determined based on the system. In the case of G, $\lambda = \lambda(\mathrm{St})$, a variable that adjusts naturally to the system as it transitions between J and I and thus has one fewer fit parameter.

When the inertial force is dominant over the hydrodynamic force (St >> 1), we find

$$\begin{aligned} \lim_{\mathrm{St/J}\to\infty} \Gamma &= \frac{2I}{\sqrt{3}} \left[6\sqrt{3}\sqrt{\frac{J}{\mathrm{St}}} + \frac{\sqrt{3}}{36}\sqrt{\frac{\mathrm{St}}{J}} + \frac{\sqrt{3}}{36}\sqrt{\frac{\mathrm{St}}{J}} W\left(-e^{-\frac{216J}{\mathrm{St}}-1}\right) \right] \\ &= \frac{2I}{\sqrt{3}} \times \frac{\sqrt{3}}{36}\sqrt{\frac{\mathrm{St}}{J}} \left[1 + W\left(-e^{-\frac{216J}{\mathrm{St}}-1}\right) \right]. \end{aligned} \tag{14}$$

Due to $\lim_{St/J\to+\infty} W(-e^{-216J/St-1}) = W(-1/e) = -1$, we apply the Taylor expansion to

$W(x)$ as $x \to -1/e$ so that $W(x) = -1 + \sqrt{2(1+ex)} - \mathcal{O}(1+ex)$ [4]. Thus,

$$\begin{aligned}\lim_{\mathrm{St/J}\to\infty} \Gamma &= \frac{2I}{\sqrt{3}}\frac{\sqrt{3}}{36}\sqrt{\frac{St}{J}}\left[\sqrt{2(1-e^{-\frac{216J}{\mathrm{St}}})} - \mathcal{O}\left(1-e^{-\frac{216J}{\mathrm{St}}}\right)\right] \\ &= \frac{2I}{\sqrt{3}}\frac{\sqrt{3}}{36}\sqrt{\frac{\mathrm{St}}{J}}\left[\sqrt{\frac{2\times 216J}{\mathrm{St}}} - \mathcal{O}\left(\frac{216J}{\mathrm{St}}\right)\right] \\ &= \frac{2I}{\sqrt{3}}\left[1 - \mathcal{O}\left(6\sqrt{3}\sqrt{\frac{J}{\mathrm{St}}}\right)\right].\end{aligned} \tag{15}$$

For the dimensionless length scale

$$\begin{aligned}\lim_{St\to\infty} G &= \frac{216J^2}{18J - I^2(1-e^{-18J/I^2})} \\ &= \frac{216J}{18 - St(1-e^{-18/St})} \\ &= \frac{216J}{18 - St(\frac{18}{St} - \frac{9\times 18}{St^2} + \frac{3\times 18^2}{St^3} - \mathcal{O}(\frac{1}{St^4}))} \\ &= \frac{216J}{\frac{9\times 18}{St} - \frac{3\times 18^2}{St^2} - \mathcal{O}(\frac{1}{St^3})} \\ &= \frac{4J\times St}{3 - \frac{18}{St} - \mathcal{O}(\frac{1}{St^2})} \\ &\approx 4I^2/3.\end{aligned} \tag{16}$$

In other words, in the limit of large St, Γ recover to the inertial number (time ratio in inertial regime), however, G transform into a square of the inertial number. When the hydrodynamic force is dominant, one obtains

$$\begin{aligned}\lim_{St/J\to+0} \Gamma &= 12J\left[1 + \frac{St}{216J} + \frac{St}{216J}W\left(-e^{-\frac{216J}{St}-1}\right)\right] \\ &= 12J,\end{aligned} \tag{17}$$

where $W(0) = 0$. The dimensionless length scale is

$$\begin{aligned}\lim_{St\to+0} G &= \frac{216J^2}{18 - St(1-e^{-18/St})} \\ &\approx \frac{216J^2}{18J} \\ &= 12J.\end{aligned} \tag{18}$$

In the limit of small St, both Γ and G have the same limiting value: $\approx 12J$. As granular materials change from a free fall regime to a viscous regime, the dimensionless numbers Γ

naturally transform from the inertial number (I) to the viscous number (J), when ignoring the constant parameter. However, G naturally recover relations from the inertial number based $(\phi_c/\phi - 1) \propto I \propto \sqrt{G}$ in the inertial regime to the viscous number based $(\phi_c/\phi - 1) \propto J^{0.5} \propto \sqrt{G}$ in the viscous regime. This is another argument to justify the choice of G as the key dimensionless parameter.

DISCRETE ELEMENT METHOD (DEM) DETAILS

The numerical simulation is implemented by the Discrete Element Method[5]. All particle positions and velocities are tracked at each instant in time. The rate changes of these quantities are calculated from the forces and moments exerted on each particle. The particles are subjected to the contact forces, lubrication forces, and drag forces:

$$m_i \frac{d^2 \boldsymbol{r}_i}{dt^2} = \sum_k \left(\boldsymbol{f}_{ik}^{c,n} + \boldsymbol{f}_{ik}^{c,t} \right) + \sum_j (\boldsymbol{f}_{ij}^{lubr,n} + \boldsymbol{f}_{ij}^{lubr,t}) + \boldsymbol{f}_i^{drag} \tag{19}$$

$$\boldsymbol{I}_i \frac{d\boldsymbol{w}_i}{dt} = \sum_k \boldsymbol{f}_{ik}^{c,t} \boldsymbol{c}^{ik} + \sum_j \boldsymbol{f}_{ij}^{lubr,t} \boldsymbol{c}^{ij} \tag{20}$$

where m_i, $\boldsymbol{r}_i$, $\boldsymbol{I}_i$,$\boldsymbol{w}_i$, are the mass, position, inertia matrix, and rotation vector of particle i, respectively. $\boldsymbol{f}_{ik}^{c,n}$, $\boldsymbol{f}_{ik}^{c,t}$ are the normal contact force, and tangential contact force subjected by particle k. $\boldsymbol{c}^{ik}$ is the vector from the center of particle i to the contact point with particle k. $\boldsymbol{f}_{ij}^{lubr,n}$ and $\boldsymbol{f}_{ij}^{lubr,t}$ are the lubrication forces in the normal and tangential direction between particle i and j. $\boldsymbol{c}^{ij}$ is the vector from the center of particle i to the point where the surface of particle i interacting with the joining vector between the center of particle i and particle j.

Contact model

The Hookean contact model is used to describe the interaction of particles. The normal and tangential contact forces $\boldsymbol{f}_{ik}^{c,n}$ and $\boldsymbol{f}_{ik}^{c,t}$ of particle i subjected by particle k is given by [5]

$$\boldsymbol{f}_{ik}^{c,n} = K_n \boldsymbol{n} \delta - c_n \Delta \boldsymbol{u}_{\boldsymbol{n}} \tag{21a}$$

$$\boldsymbol{f}_{ik}^{c,t} = \min(|K_t \boldsymbol{x}_{\boldsymbol{t}}|, |\mu_p \boldsymbol{f}_{ik}^{c,n}|) \frac{\boldsymbol{x}_{\boldsymbol{t}}}{|x_t|}. \tag{21b}$$

where δ is the overlap of the contact particles a and b), $K_n = \frac{2k_n^a k_n^b}{k_n^a + k_n^b}$ and $K_t = \frac{2k_t^a k_t^b}{k_t^a + k_t^b}$ are the effective normal and tangential stiffness which are calculated by the stiffness of the contact particles (k_n^a,k_t^a are the normal and tangential stiffness of particle a, and k_n^b,k_t^b are the normal and tangential stiffness of particle b), $\boldsymbol{n}$ is the unit normal vector pointing from the centroid of particle a to centroid of particle b, and $\boldsymbol{\Delta u_n}$ is the relative normal velocity. Here, the normal viscous coefficient is

$$c_n = \frac{-\ln e_n \sqrt{2\bar{m}K_n}}{\sqrt{\pi^2 + (\ln e_n)^2}} \tag{22}$$

where e_n is the restitution coefficient and the equivalent mass, $\bar{m} = \frac{2m_a m_b}{m_a + m_b}$,$m_a$ and m_b are the mass of each particle. $\boldsymbol{x_t}$ is the relative displacement of contact points in the tangential direction, and μ_p is the frictional coefficient between contacting particles. The simulation parameters are listed in Table.I.

TABLE I. Simulation parameters in the present work

k_n(dyn/cm)	k_t(dyn/cm)	μ_p	e_n
5e7	1e7	0.3	0.2

Hydrodynamic forces

During the simple shear simulation, the particles are subjected to both drag and lubrication forces. The drag force for particle i is

$$\boldsymbol{f}_i^{drag} = 3\pi\eta_f d \left[\boldsymbol{u}^f(z_i) - \boldsymbol{u}_i^p\right], \tag{23}$$

where $\boldsymbol{u}^f$ and $\boldsymbol{u}^p$ are the velocities of the fluid and the particle. Further, we assume that the fluid velocity is linearly distributed in the z-direction inspired by the work of Ref.[1]. It needs to be mentioned that the drag force in the present work is based on the condition of a low Reynolds number in the dense granular flow. The lubrication force [6] between particle i and j in the normal and tangential directions are

$$\begin{aligned} \boldsymbol{f}_{ij}^{lubr,n} &= 6\pi\eta_f R_{\text{eff}}^2 \frac{\boldsymbol{v}_n^{rel}}{\delta_g}, \quad \text{and} \\ \boldsymbol{f}_{ij}^{lubr,t} &= 6\pi\eta_f R_{\text{eff}}^2 \boldsymbol{v}_t^{rel} \left[\frac{8}{15}\ln\frac{R_{\text{eff}}}{\delta_g} + 0.9588\right], \end{aligned} \tag{24}$$

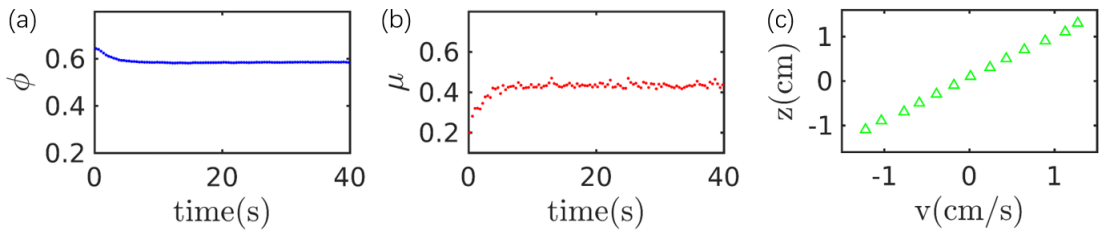

FIG. 3. Samples of (a) the solid fraction ϕ of the granular assembly, and (b) the apparent friction coefficient μ of the granular assembly for the simulation under fluid. (c) velocity distribution of particles in the Z direction at time=40s to illustrate the approach of the system to a steady state when $v(z)$ is linear and μ and ϕ are unchanging.

where $R_{\text{eff}} = [2(d_i^{-1} + d_j^{-1})]^{-1}$, d_i and d_j are the diameters of particles i and j. δ_g is the distance between the surfaces of particles i and j. The cut-off length of δ_g is R_{eff}. $\boldsymbol{v}_n^{rel}$ and $\boldsymbol{v}_t^{rel}$ are the relative velocities between the nearest points of two particles in the normal and tangential direction.

Figs.3(a)(b) plots ϕ and μ versus the simulation time, and fig.3(c) plots the velocity distribution in the Z direction at the time= 40s in our numerical simulation. We identify that the granular flow is in a quasi-steady state when ϕ and μ do not change and the velocity distribution is linear in the Z direction.

REGRESSION ANALYSIS FOR FITTING EXPRESSIONS OF μ AND ϕ

We performed regression analysis to find the best fits for each rheological expression (μ and ϕ) and to evaluate their performance quantitatively. To present the details of this in the following, we represent the original data by X_o and the predicted value from each fitting expression by X_p. Then, for the choice of model fit parameters, we calculated and minimized the $R-$squared value R^2:

$$R^2 = 1 - \frac{SSE}{SST} \tag{25a}$$

$$SSE = \sum_{i=1:N} (X_{o,i} - X_{p,i}) \tag{25b}$$

$$SST = \sum_{i=1:N} (X_{o,i} - \bar{X})^2 \tag{25c}$$

SSE is the sum of squares of residuals, TSS is the total sum of squares, N is the number of samples, and $\bar{X}$ is the mean of the sample. Then to evaluate the relative effectiveness of

each fit, we calculated the Root-mean-squared value, that is, the square root of the average variance of the data about the fit:

$$RMS = \sqrt{\frac{1}{N}\sum_{i=1:N}(X_{o,i} - X_{p,i})^2} \tag{26}$$

The outcome for fitting our data to μ and ϕ using K and G is given in Table 2 of the main text.

UNIVERSAL COLLAPSE AND MATERIAL PROPERTIES: CRITICAL APPARENT FRICTION AND SOLID FRACTION

As previously shown by some of the co-authors of this paper in Ref. [7], we minimize the residuals between our data and the fits for μ and ϕ:

$$\mu = \mu_1 + \frac{\mu_2 - \mu_1}{1 + \mathcal{Q}_G/\sqrt{G}} \tag{27a}$$

$$\phi = \frac{\phi_c}{1 + b_G \times \sqrt{G}} \tag{27b}$$

Then we used the fit parameters $\mathcal{Q}_G$, b_G determined from fitting our data sets for all other data sets by plotting a reworked form of Eqns. 27aand 27b:

$$\frac{\mu - \mu_1}{\mu_2 - \mu_1} = \frac{1}{1 + \mathcal{Q}_G/\sqrt{G}} \tag{28}$$

was universal for all data. Similarly, using the fit parameters ϕ_c and b_G and rearranging the expression for $\phi(G(\mathrm{St}))$ we find a universal fit in:

$$\frac{\phi_c - \phi}{\phi} = b_G \times \sqrt{G} \tag{29}$$

The critical solid fraction and apparent friction in different conditions are listed in Tables.II, and III.

DATA COLLAPSE FOR 2-D CONDITION

The 2D LBM-DEM simulation data obtained from Ref.[12] is used here to verify our rheological law. The viscosity of fluid η_f, shear rate $\dot{\gamma}$, confining pressure P, and relative density ρ_s/ρ_f in the simulation are in wide ranges as shown in Table.IV. As shown in Fig.4

TABLE II. Critical apparent friction and solid fraction for the present simulation.

η_f(cP)	Dry	0.1	1	20	100	1000
ϕ_c	0.6075	0.6075	0.6075	0.6075	0.6075	0.6075
μ_1	0.34	0.34	0.34	0.34	0.34	0.34
μ_2	1.49	1.49	1.49	1.49	1.49	1.49
α	0.5	0.5	0.5	0.5	0.5	0.5

TABLE III. Critical apparent friction and solid fraction for the previous investigations[8–11]

η_f(cP)	Air[8]	1[8]	11[8]	20[8]	50[8]	86[8]	Dry[9]	Dry[10]	31[11]
ϕ_c	0.596	0.586	0.615	0.618	0.615	0.614	-	0.587	0.585
μ_1	0.39	0.4065	0.31	0.308	0.3	0.29	0.397	0.36	0.29
μ_2	1.73	1.688	1.215	1.74	2.25	2.9	1.22	1.43	3.12

and Fig.5, the characteristic length scale G shows a good collapse of the solid fraction ϕ and the apparent friction coefficient μ, which validates our work.

* manteng@westlake.edu.cn

† s.Torres@westlake.edu.cn

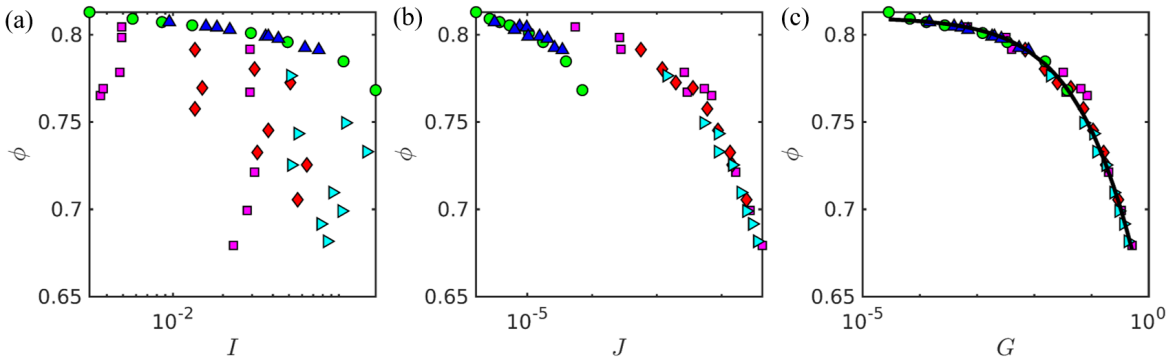

FIG. 4. Simulation data from Ref.[12] of 2-D submerged conditions with different viscosities. We plot μ as a function of (a) I, (b) J, (c) $\mathcal{L}/l = G$. The solid line is given by Eqn.24b, $\phi_c = 0.81$, $b = 0.276$.

TABLE IV. Input parameters in the Ref.[12]

η_f	$\dot{\gamma}$	P	ρ_s/ρ_f
$\eta_w \sim 2500\eta_w$	$0.28 \sim 5.6$ s^{-1}	$20 \sim 120$ Pa	$0.5 \sim 3$

[a] η_w is the model fluid viscosity.

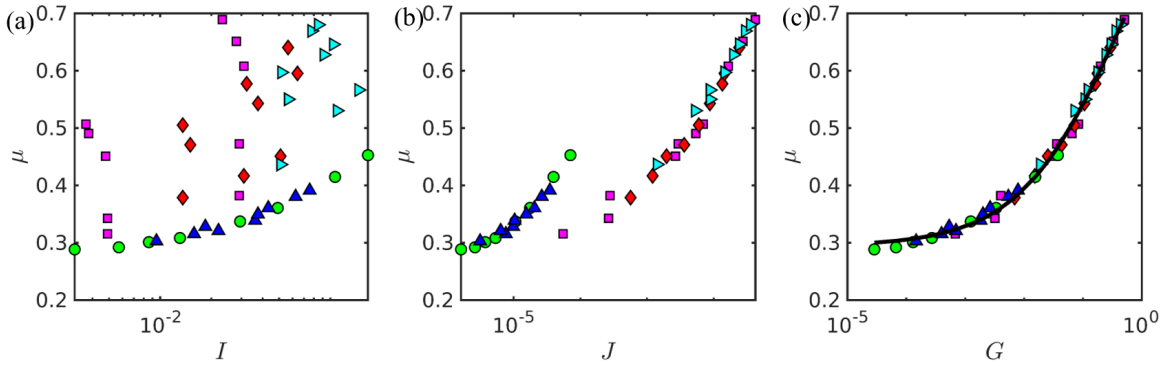

FIG. 5. Simulation data from Ref.[12] of 2-D submerged conditions with different viscosities. We plot ϕ as a function of (a) I, (b) J, (c) $\mathcal{L}/l = G$. The solid line is given by Eqn.24a, $\mu_1 = 0.2936$, $\mu_1 = 1.074$, $\mathcal{Q} = 0.674$.

[1] M. Trulsson, B. Andreotti, and P. Claudin, Transition from the viscous to inertial regime in dense suspensions, Physical Review Letters **109**, 118305 (2012).

[2] T. C. Scott, R. Mann, and R. E. Martinez Ii, General relativity and quantum mechanics: towards a generalization of the lambert w function a generalization of the lambert w function, Applicable Algebra in Engineering, Communication and Computing **17**, 41 (2006).

[3] C. Cassar, M. Nicolas, and O. Pouliquen, Submarine granular flows down inclined planes, Physics of fluids **17**, 103301 (2005).

[4] D. Veberič, Lambert w function for applications in physics, Computer Physics Communications **183**, 2622 (2012).

[5] P. A. Cundall and O. D. Strack, A discrete numerical model for granular assemblies, Geotechnique **29**, 47 (1979).

[6] A. J. Goldman, R. G. Cox, and H. Brenner, Slow viscous motion of a sphere parallel to a plane wall—i motion through a quiescent fluid, Chemical engineering science **22**, 637 (1967).

[7] T. Man, P. Zhang, Z. Ge, S. A. Galindo-Torres, and K. M. Hill, Friction-dependent rheology of dry granular systems, Acta Mechanica Sinica **39**, 1 (2023).

[8] F. Tapia, M. Ichihara, O. Pouliquen, and E. Guazzelli, Viscous to inertial transition in dense granular suspension, Physical Review Letters **129**, 078001 (2022).

[9] S. B. Savage, The mechanics of rapid granular flows, Advances in Applied Mechanics **24**, 289 (1984).

[10] E. Azéma and F. Radjaï, Internal structure of inertial granular flows, Phys. Rev. Lett. **112**, 078001 (2014).

[11] F. Boyer, É. Guazzelli, and O. Pouliquen, Unifying suspension and granular rheology, Physical Review Letters **107**, 188301 (2011).

[12] L. Amarsid, J.-Y. Delenne, P. Mutabaruka, Y. Monerie, F. Perales, and F. Radjai, Viscoinertial regime of immersed granular flows, Physical Review E **96**, 012901 (2017).